

# A patterned anisotropic nanofluidic sieving structure for continuous-flow separation of DNA and proteins

JIANPING FU<sup>1\*</sup>, RETO B. SCHOCH<sup>2,3\*</sup>, ANNA L. STEVENS<sup>3</sup>, STEVEN R. TANNENBAUM<sup>3</sup>  
AND JONGYOON HAN<sup>2,3†</sup>

<sup>1</sup>Department of Mechanical Engineering, Massachusetts Institute of Technology, Cambridge, Massachusetts 02139, USA

<sup>2</sup>Department of Electrical Engineering and Computer Science, Massachusetts Institute of Technology, Cambridge, Massachusetts 02139, USA

<sup>3</sup>Biological Engineering Division, Massachusetts Institute of Technology, Cambridge, Massachusetts 02139, USA

\*These authors contributed equally to this work

†e-mail: jyhan@mit.edu

Published online: 5 February 2007; doi:10.1038/nnano.2006.206

Microfabricated regular sieving structures hold great promise as an alternative to gels to improve the speed and resolution of biomolecule separation. In contrast to disordered porous gel networks, these regular structures also provide well defined environments ideal for the study of molecular dynamics in confining spaces. However, the use of regular sieving structures has, to date, been limited to the separation of long DNA molecules, however separation of smaller, physiologically relevant macromolecules, such as proteins, still remains a challenge. Here we report a microfabricated anisotropic sieving structure consisting of a two-dimensional periodic nanofluidic filter array. The designed structural anisotropy causes different-sized or -charged biomolecules to follow distinct trajectories, leading to efficient separation. Continuous-flow size-based separation of DNA and proteins, as well as electrostatic separation of proteins, was achieved, demonstrating the potential use of this device as a generic molecular sieving structure for an integrated biomolecule sample preparation and analysis system.

Efficient methods for separating and purifying biomolecules from a complex mixture are of the utmost importance in biology and biomedical engineering. Currently, nucleic acids and proteins are routinely separated based on size by gel filtration chromatography or by gel electrophoresis<sup>1,2</sup>. Both techniques use gelatinous materials consisting of a cross-linked, three-dimensional pore network, where the sieving interaction with the migrating macromolecules determines the efficiency of separation<sup>3,4</sup>. Both gel-based techniques represent the current standard for size-based macromolecule separation. However, the disadvantages of poor separation resolution in gel filtration chromatography and difficult sample recovery with gel electrophoresis make neither method optimal in separating complex mixtures for downstream analysis<sup>1</sup>. Liquid and solid gelatinous materials have also been integrated in microchip-based systems for rapid separation of biomolecules (such as DNA, proteins and carbohydrates) with high resolution<sup>5–7</sup>. However, the foreign sieving matrices have intrinsic difficulties for the integration of automated multistep bioanalysis microsystems. Furthermore, these microchip-based systems only process a small sample plug in a batch processing mode with low overall volume throughput, which presents their use in preparatory separation.

Recently, there has been great interest in switching from disordered porous gel media to patterned regular sieving structures, either by colloidal templating of self-assembled bead arrays<sup>8,9</sup> or by microfabrication techniques<sup>10–15</sup>. Although significantly more efficient than gels in terms of separation speed and resolution, these regular sieving structures still largely resemble gels in the

sense that separation is achieved by repeated sieving through multiple, identical ‘pores’. More recently, microfabricated asymmetric obstacle courses have been used to continuously separate macromolecules either by diffusion<sup>16,17</sup> or by asymmetric bifurcation of laminar flow<sup>18</sup>. This later work took advantage of the asymmetric interaction of macromolecules with the device geometries, which enabled these novel separation mechanisms. However, the regular sieving structures discussed so far have proven efficacious only for separation of long DNA molecules and microspheres, and their applicability to smaller, physiologically relevant macromolecules remains questionable<sup>19,20</sup>, which clearly limits progress towards a future integrated bioanalysis system.

Here we report a unique molecular sieving structure design, called the anisotropic nanofilter array<sup>21</sup> (ANA), and its implementation for continuous-flow separation of DNA and proteins based on either size or charge. The designed structural anisotropy of the ANA is critical to continuous-flow separation. This is not readily possible with a random isotropic sieving medium such as gels, liquid gels or ampholytes. Moreover, the ANA allows for various sieving mechanisms (for example, Ogston sieving<sup>22–24</sup>, entropic trapping<sup>25–28</sup> and electrostatic sieving<sup>29,30</sup>) to take effect in the separation of biomolecules covering very broad biological size ranges and based on different molecular properties, which is a clear advantage over the aforementioned conventional and non-conventional techniques. The continuous-flow operation of the ANA further permits continuous harvesting of purified biomolecules for downstream analysis, rendering the ANA a

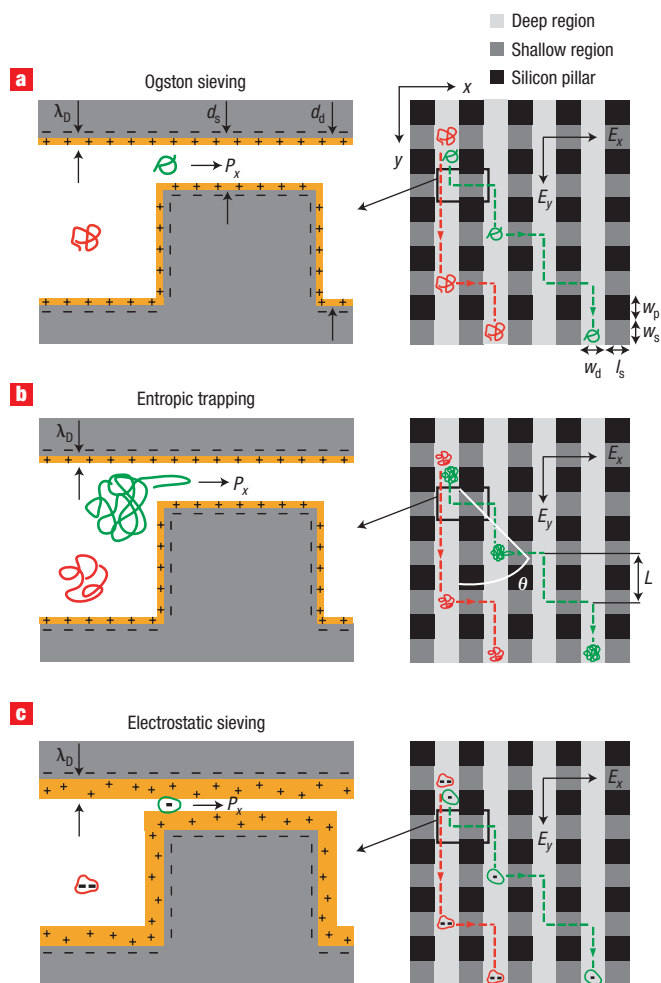


**Figure 1** Schematic showing negatively charged macromolecules assuming bidirectional motion in the ANA under the influence of two orthogonal electric fields  $E_x$  and  $E_y$ . Nanofilters (width,  $w_s$ ; length,  $l_s$ ; depth,  $d_s$ ) arranged in rows are separated by deep channels (width,  $w_d$ ; depth,  $d_d$ ). Rectangular pillars (width,  $w_p$ ; length,  $l_p$ ) serve as supporting structures to prevent the collapse of the top ceiling. **a, b**, When the Debye length  $\lambda_D \ll d_s$  (Debye layer highlighted in yellow), the steric exclusion effect dictates jump dynamics. For Ogston sieving (**a**), smaller-sized molecules (in green) are preferred for nanofilter passage, resulting in a greater nanofilter jump passage rate  $P_x$ . In entropic trapping (**b**), the longer linear molecules (in green) assume a greater probability of hernia formation and thus a greater passage rate  $P_x$ . **c**, Electrostatic sieving becomes dominant when  $\lambda_D \approx d_s$ . Similar sized globular molecules with a lower negative net charge (in green) experience lesser electrostatic repulsion when crossing the negatively charged nanofilter, resulting in a greater passage rate  $P_x$ . The mean drift distance  $L$  between two consecutive nanofilter crossings plays a determinant role for the migration trajectory, with a shorter  $L$  leading to a larger stream deflection angle  $\theta$ , where  $\theta$  is defined with respect to the positive  $y$  axis.

promising generic sieving structure for an integrated biomolecule sample preparation and analysis system.

## RESULTS

### DESIGN OF THE ANA

The design of the ANA consists of a two-dimensional periodic nanofilter array (Fig. 1). The separation mechanism of the ANA

relies on different sieving characteristics along two orthogonal directions within the ANA, which are set perpendicular and parallel to the nanofilter rows (indicated as the  $x$  and  $y$  axes, respectively, in Fig. 1). Upon application of an electric field  $E_y$  along the  $y$  axis, negatively charged macromolecules are driven into the nanofilter array following the direction of either the electrophoretic force (electrophoresis) or hydrodynamic drag force from electro-osmotic flow (electro-osmosis) (see Methods). An orthogonal electric field  $E_x$  is superimposed along the  $x$  axis across the nanofilters, and this field selectively drives the drifting macromolecules in the deep channel to jump across the nanofilter in the positive  $x$  direction to the adjacent deep channel.

Molecular crossings of the nanofilter under the influence of  $E_x$  can be described as biased, thermally activated jumps across free energy barriers at the nanofilter threshold<sup>28,31</sup>, and these free energy barriers depend on both steric and electrostatic interactions between charged macromolecules and charged nanofilter walls<sup>30</sup>. At high ionic strength where the Debye length  $\lambda_D$  is negligible compared to the nanofilter shallow region depth  $d_s$ , electrostatic interactions between charged macromolecules and charged nanofilter walls are largely screened. The energy barriers are therefore solely determined by the configurational or conformational entropy loss within the constriction due to steric exclusion (a purely steric limit)<sup>28,31,32</sup>. For biomolecules with diameters smaller than the nanofilter constriction (Ogston sieving), the steric energy barrier has been shown to favour DNA and proteins with a smaller size for passage<sup>24</sup> (Fig. 1a), resulting in a greater jump passage rate  $P_x$  for smaller molecules. Therefore, in Ogston sieving, smaller molecules travel a shorter mean characteristic drift distance  $L$  in the deep channels between two consecutive nanofilter crossings, leading to a larger stream deflection angle  $\theta$ .

For macromolecules with diameters greater than the nanofilter constriction size, passage requires the molecules to deform and form hernias at the cost of their internal conformational entropy (entropic trapping)<sup>9,12</sup>. A previous study on long DNA molecules trapped at a similar nanofluidic constriction showed that the steric energy barrier for DNA escape depends solely on the inverse of the electric field strength ( $\sim 1/E_x$ ) (ref. 28). Furthermore, longer molecules have a larger surface area contacting the constriction and thus have a greater probability of forming the hernias that initiate the escape process (in other words, they have a higher escape attempt frequency)<sup>33</sup> (Fig. 1b). Therefore, in entropic trapping, longer molecules have a greater jump passage rate  $P_x$ , resulting in a larger deflection angle  $\theta$ .

For low-ionic-strength solutions where the Debye length  $\lambda_D$  becomes comparable to the nanofilter shallow region depth  $d_s$ , repulsive electrostatic interactions between negatively charged biomolecules and like-charged nanofilter walls become prominent and start to dictate jump dynamics across the nanofilter (Fig. 1c)<sup>29,30</sup>. The electric potential remains negative in the entire nanochannel, resulting in an electrostatic exclusion of negatively charged molecules. Such electrostatic effects on the partitioning of macromolecules through nanopores have been well studied in membrane science<sup>29,30</sup>, and have recently been applied for pH-controlled diffusion of proteins across a nanochannel<sup>34</sup>. Therefore, similar sized biomolecules bearing a lower net charge are energetically favoured for passage through the nanofilter, resulting in a greater jump passage rate  $P_x$  and a larger deflection angle  $\theta$ .

We fabricated a silicon-based device that incorporates the ANA as the sieving structure (Fig. 2). The ANA contains nanofilters with a constriction size of 55 nm ( $d_s$ ) and a width of 1  $\mu\text{m}$  ( $w_s$ ). Deep channels separating the nanofilter rows are 1  $\mu\text{m}$

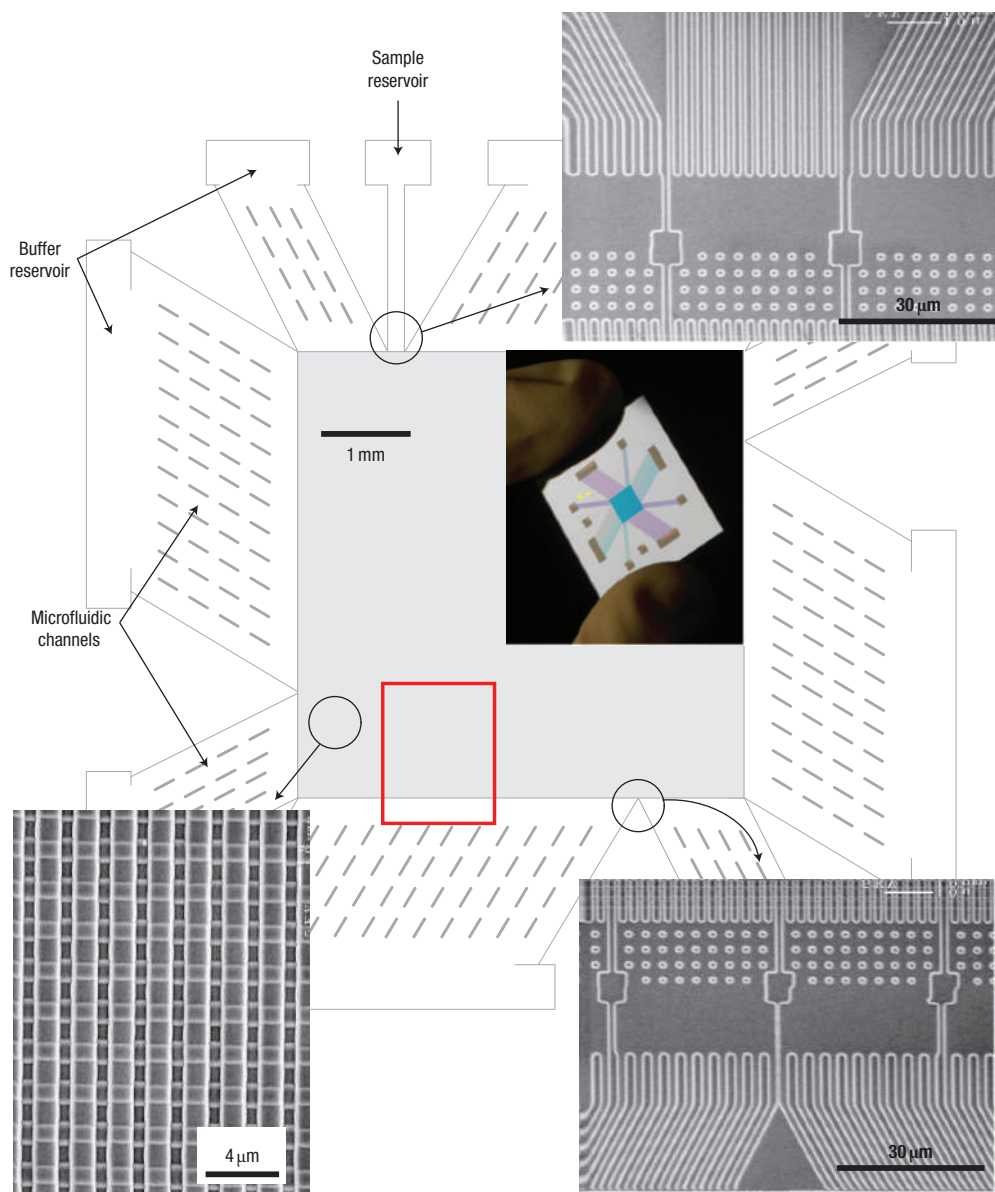


**Figure 2** Structure of the microfabricated device incorporating the ANA. Scanning electron microscopy images show details of different device regions (clockwise from top right: sample injection channels, sample collection channels and ANA). The inset shows a photograph of the thumbnail-sized device. The rectangular ANA is 5 mm × 5 mm, and nanofilters ( $w_s = 1 \mu\text{m}$ ,  $l_s = 1 \mu\text{m}$ ,  $d_s = 55 \text{ nm}$ ) are spaced by  $1 \mu\text{m} \times 1 \mu\text{m}$  square silicon pillars. Deep channels are  $1 \mu\text{m}$  wide ( $w_d$ ) and 300 nm deep ( $d_d$ ). Injection channels connected to the sample reservoir (1 mm from the ANA top left corner) inject biomolecule samples as a 30- $\mu\text{m}$ -wide stream. The red rectangle highlights the area in which the fluorescence photographs in Fig. 3 were taken.

wide ( $w_d$ ) and 300 nm deep ( $d_d$ ). The initial biomolecule stream is continuously injected into the deep channels on the top left of the device. The fractionated biomolecule streams are collected at intervals along the opposite edge. Microfluidic channels surrounding the ANA connect to fluid reservoirs, where voltages are applied. The microfluidic channels provide sample loading and collection ports, and further act as electric-current injectors to create uniform electric fields  $E_x$  and  $E_y$  over the ANA structure<sup>13,35</sup>.

#### OGSTON SIEVING OF SHORT DNA MOLECULES

To demonstrate explicitly the steric sieving effect of the ANA, we first injected a low-molecular-weight (MW) DNA ladder sample

(a mixture of DNA strands of different lengths that can be used as a standard when analysing products of the polymerase chain reaction, the PCR marker) in Tris-Borate-EDTA (TBE) 5× buffer (0.445 M Tris-Borate, 10 mM EDTA, pH ~8.3) under a broad range of field conditions (Fig. 3). As TBE 5× buffer has an equivalent ionic strength of ~130 mM (ref. 36) with a corresponding Debye length  $\lambda_D$  of about 0.84 nm ( $\ll d_s = 55 \text{ nm}$ ), steric interactions dominate the jump dynamics. The PCR marker contains five different DNA fragments of sizes ranging from 50 to 766 base pairs (bp). As the persistence length of DNA is about 50 nm (about the contour length of 150-bp DNA; ref. 37), the PCR marker fragments appear relatively straight, and are recognizable as rigid, rod-like molecules with an end-to-end

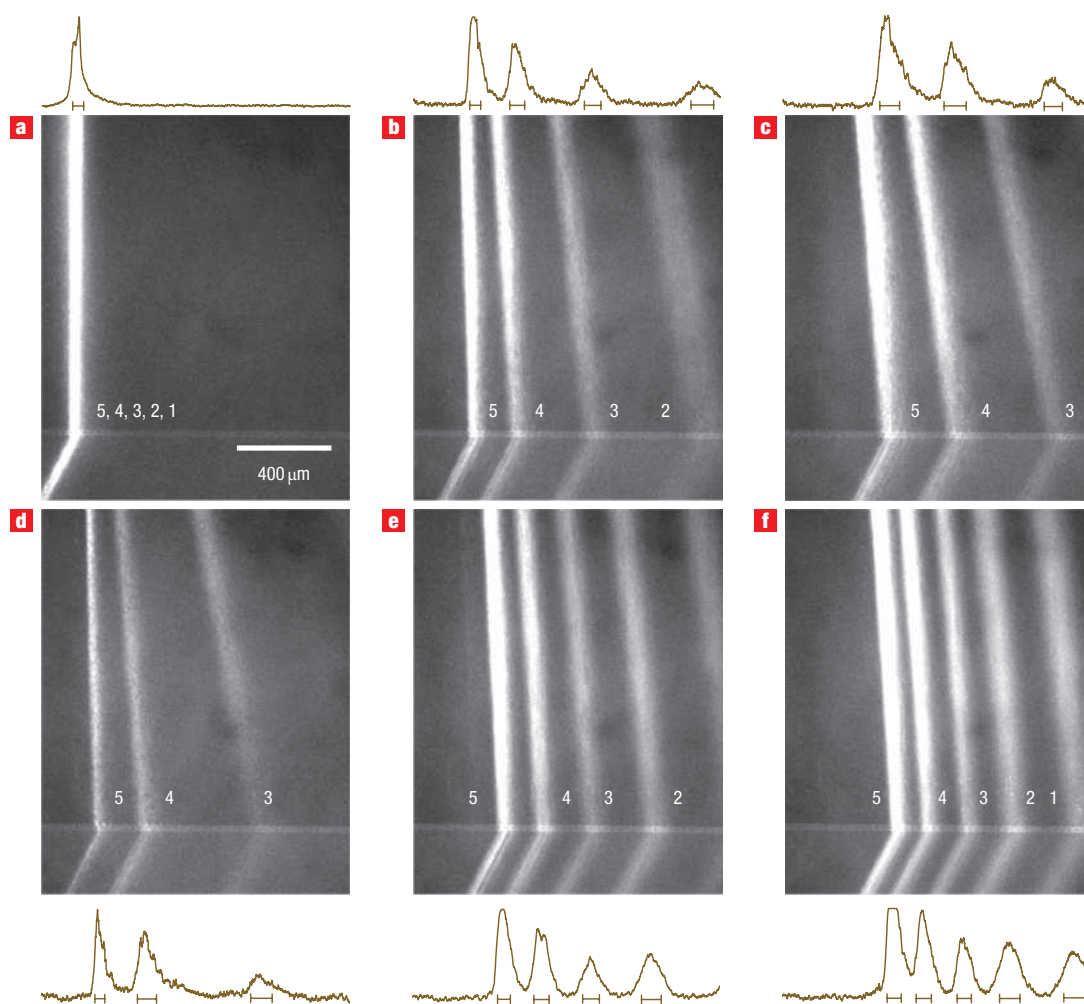


**Figure 3** Ogston sieving of short DNA (the PCR marker) through the ANA. Fluorescence photographs of the PCR marker stream pattern were taken in the area highlighted by the red rectangle in Fig. 2. **a**, Only  $E_y$  is applied, where  $E_y = 25 \text{ V cm}^{-1}$ . **b**,  $E_x = 35 \text{ V cm}^{-1}$  and  $E_y = 25 \text{ V cm}^{-1}$ . **c**,  $E_x = 60 \text{ V cm}^{-1}$  and  $E_y = 25 \text{ V cm}^{-1}$ . **d**,  $E_x = 35 \text{ V cm}^{-1}$  and  $E_y = 12.5 \text{ V cm}^{-1}$ . **e**,  $E_x = 35 \text{ V cm}^{-1}$  and  $E_y = 50 \text{ V cm}^{-1}$ . **f**,  $E_x = 35 \text{ V cm}^{-1}$  and  $E_y = 75 \text{ V cm}^{-1}$ . The band assignments are 50 bp (1), 150 bp (2), 300 bp (3), 500 bp (4) and 766 bp (5). Fluorescence intensity profiles (of arbitrary units) were measured at the ANA bottom edge. The bars under the peaks are centred at the means and label the stream widths ( $\pm$ s.d.).

distance of between 16 nm and 150 nm (refs 31 and 38). The entry into the confining nanofilter can only be realized if the rod-like DNA molecules are properly positioned and orientated without overlapping the wall, which limits the configurational freedom and creates an entropic barrier (Ogston sieving)<sup>2,31,39</sup>. Figure 3a–f shows six fluorescence photographs of the PCR marker stream pattern in the ANA when horizontal and vertical fields of different values are applied. The horizontal field  $E_x$  quickly deflects DNA fragments according to their molecular weights (size), with the stream deflection angle  $\theta$  and the stream width depending on the exact field conditions (see Supplementary Information, Video S1). Increasing the horizontal field  $E_x$  resulted in larger deflection angles as well as wider spreading of the streams.

In Ogston sieving, the nanofilter jump passage rate  $P_x$  for short DNA of a base-pair number  $N$  can be calculated based on equilibrium partitioning theory and Kramer's rate theory<sup>31</sup>. In the limit of low field, the passage rate  $P_x$  is proportional to  $E_x^2 K/N$ , where  $K$  is the DNA equilibrium partitioning coefficient across

the nanofilter<sup>31</sup>. Therefore, increasing  $E_x$  enhances the jump passage rate  $P_x$ , leading to a shorter drift distance  $L$  and thus a larger deflection angle  $\theta$ . Based on the calculation of  $P_x$ , we have constructed a coarse-grained kinetic model to explain the field-dependent stream deflection angle  $\theta$  (see Supplementary Information, text and Fig. S1).

The vertical electric field  $E_y$  also affects the deflection angle  $\theta$ . As  $E_y$  was raised from  $12.5 \text{ V cm}^{-1}$  to  $75 \text{ V cm}^{-1}$  at fixed  $E_x = 35 \text{ V cm}^{-1}$  (Fig. 3d–f), the DNA stream pattern became more focused, with shorter DNA fragments (50 bp, 150 bp) shifting towards the negative  $x$ -direction and longer DNA fragments (300 bp, 500 bp, 766 bp) shifting towards the positive. A greater vertical field  $E_y$  shortens the time for DNA to explore the transition through a nanofilter threshold, which explains the behaviour of short DNA with increased  $E_y$ . The long DNA fragments shifted with  $E_y$  in ways that are not yet fully understood, although the changes were reproducible with  $E_y$  up to  $125 \text{ V cm}^{-1}$ . We suspect this phenomenon might be due to the slight non-uniformity of  $E_x$  and  $E_y$  over the ANA.

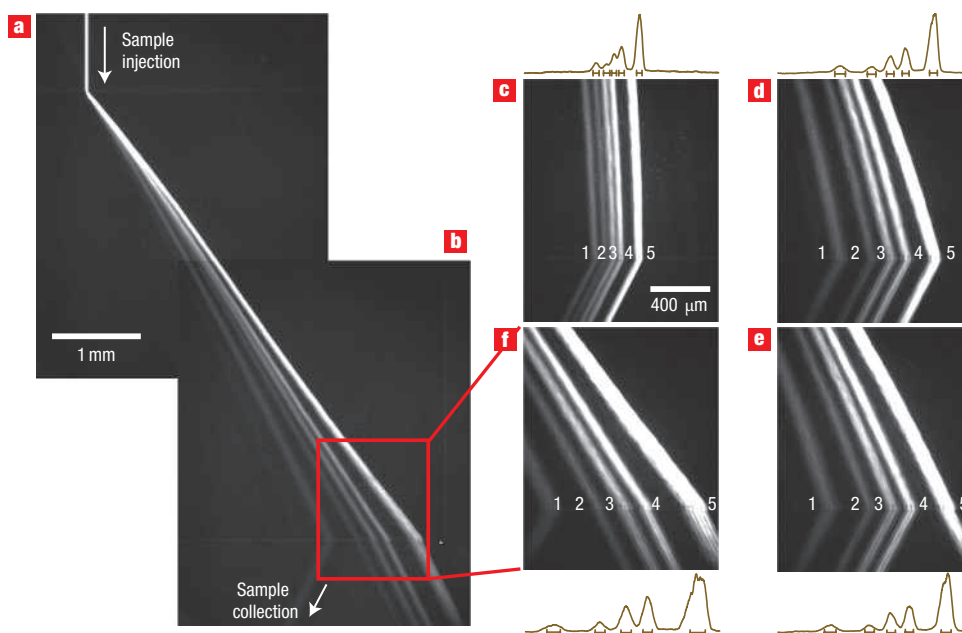


**Figure 4** Entropic trapping of long DNA (the  $\lambda$  DNA–Hind III digest) through the ANA. Fluorescent photographs show separation of  $\lambda$  DNA–Hind III digest with different electric field conditions. **a,b,f**,  $E_x = 185 \text{ V cm}^{-1}$  and  $E_y = 100 \text{ V cm}^{-1}$ . **c**,  $E_x = 50 \text{ V cm}^{-1}$  and  $E_y = 100 \text{ V cm}^{-1}$ . **d**,  $E_x = 145 \text{ V cm}^{-1}$  and  $E_y = 100 \text{ V cm}^{-1}$ . **e**,  $E_x = 170 \text{ V cm}^{-1}$  and  $E_y = 100 \text{ V cm}^{-1}$ . The band assignments are 2,322 bp (1), 4,361 bp (2), 6,557 bp (3), 9,416 bp (4), 23,130 bp (5). Fluorescence intensity profiles were measured at the ANA bottom edge. The bars under the peaks are centred at the means and label the stream widths ( $\pm$ s.d.).

#### ENTROPIC TRAPPING OF LONG DNA MOLECULES

The ANA can separate long DNA molecules based on the entropic trapping mechanism. We prepared a mixture of long DNA molecules (the  $\lambda$  DNA–Hind III digest) in TBE 5 $\times$  buffer, which contains six DNA fragments with sizes ranging from 2,027 bp to 23,130 bp, and corresponding equilibrium (unconfined) radii of gyration  $R_g$  ranging from  $\sim$ 140 nm to 520 nm (ref. 40). These  $R_g$  values are useful estimates of the spherical DNA size, and they are all greater than the nanofilter constriction depth  $d_s$ . Therefore, the nanofilter jump dynamics necessarily involves deformation and hernia nucleation (that is, entropic trapping).

With application of  $E_x = 185 \text{ V cm}^{-1}$  and  $E_y = 100 \text{ V cm}^{-1}$ , the  $\lambda$  DNA–Hind III digest was separated in less than 1 min with baseline resolution (Fig. 4a, b and Supplementary Information, Video S2; note that the shortest 2,027 bp fragment was too dim for clear visualization in Fig. 4, but with higher gain setting and longer exposure time of the charge-coupled device (CCD), the 2,027 bp fragment was identified to be baseline separated with the others). A closer look at Video S2 reveals that, as expected, longer DNA fragments followed more deflected migration trajectories than shorter ones, a clear distinction of entropic trapping from Ogston sieving. The streams of  $\lambda$  DNA–Hind III digest followed more deflected and resolved trajectories as  $E_x$  was increased (Fig. 4c–f). This observation is consistent with the argument that increased  $E_x$  lowers the activation energy barrier, leading to a higher jump passage rate  $P_x$  (ref. 28).

#### SIZE- OR CHARGED-BASED SEPARATION OF PROTEINS WITH THE ANA

Mixtures of proteins under both native (Fig. 5) and denaturing conditions (see Supplementary Information, Fig. S2) have been separated by the ANA based on either size or charge, depending on buffer ionic strength. As proof of concept, we investigated the following various standard proteins dissolved in either TBE 5 $\times$  or TBE 0.05 $\times$  (4.45 mM Tris–Borate, 0.1 mM EDTA) buffer, both

at pH 9.6: lectin from *Lens culinaris* (lentil) (MW  $\sim$ 49 kDa, isoelectric point (pI, characteristic pH value at which proteins exhibit zero net charge)  $\sim$ 8.0–8.8); streptavidin (MW  $\sim$ 52.8 kDa, pI of  $\sim$ 5–6); B-phycoerythrin (MW  $\sim$ 240 kDa, pI of  $\sim$ 4.2–4.4); and fibrinogen (MW  $\sim$ 340 kDa, pI of  $\sim$ 5.5). Under the horizontal field  $E_x = 100 \text{ V cm}^{-1}$  and the vertical field  $E_y = 50 \text{ V cm}^{-1}$ , a mixture of lectin, B-phycoerythrin and fibrinogen was driven through the ANA at TBE 5 $\times$ .

The three proteins were clearly separated into three distinct streams according to their molecular weights, and non-specific adsorption on the ANA was not significant, possibly due to electrostatic repulsion from the like charged hydrophilic ANA walls<sup>41</sup> (Fig. 5a–c). The stream deflection angles of lectin, B-phycoerythrin and fibrinogen are about  $30.21^\circ$ ,  $27.88^\circ$  and  $24.04^\circ$ , respectively. The resolution values  $R_s$  for lectin and B-phycoerythrin at 1.5 mm and 5 mm (extrapolated, see Methods) from the injection point are 0.33 and 0.47, respectively, and for B-phycoerythrin and fibrinogen, the  $R_s$  values are 0.95 and 1.24, respectively. In all the experiments, lectin was deflected most, followed by B-phycoerythrin and then fibrinogen, suggesting Ogston sieving to account for the jump dynamics. Further increasing  $E_x$  resulted in larger lateral separation and broader lateral dispersion of the streams. Similar separation experiments with sodium dodecyl sulphate (SDS)–protein complexes at TBE 5 $\times$  also supported Ogston sieving for the differential jump dynamics across nanofilters (see Supplementary Information, Fig. S2).

Electrostatic sieving in the ANA was demonstrated at TBE 0.05 $\times$  by separating two proteins, lectin and streptavidin, under native conditions. The proteins have similar molecular weights and a relatively large difference in pI values. No separation of these two proteins was observed at TBE 5 $\times$  (Fig. 5d), which excludes the possibility of size-based separation. However, at TBE 0.05 $\times$  (equivalent ionic strength of 1.3 mM (ref. 36) and a

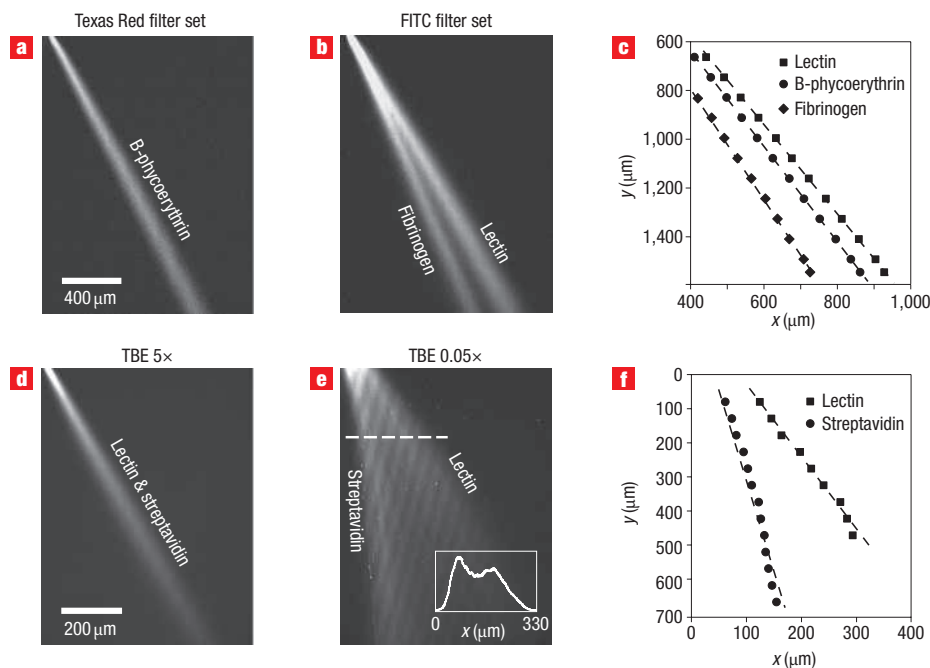


**Figure 5** Continuous-flow separation of proteins through the ANA. Proteins are driven through the ANA following electro-osmosis. With TBE 5 $\times$ , the separation time was within a few minutes; with TBE 0.05 $\times$ , the separation time was of the order of tens of seconds. **a, b**, Fluorescence photographs showing separation of lectin, B-phycoerythrin and fibrinogen at TBE 5 $\times$  with  $E_x = 100 \text{ V cm}^{-1}$  and  $E_y = 50 \text{ V cm}^{-1}$ . Images **a** and **b** were taken for the same ANA area (**a** with a Texas Red filter set, **b** with a FITC filter set). **c**, Maximum fluorescence intensity along the streams measured for both **a** and **b** as a function of  $x$  and  $y$ . **d**, No separation was observed for lectin and streptavidin at TBE 5 $\times$  with  $E_x = 150 \text{ V cm}^{-1}$  and  $E_y = 75 \text{ V cm}^{-1}$ . **e**, Fluorescence photograph shows separation of lectin and streptavidin at TBE 0.05 $\times$  with  $E_x = 250 \text{ V cm}^{-1}$  and  $E_y = 75 \text{ V cm}^{-1}$ . The inset shows the fluorescence intensity profile scanned along the dashed line (at  $y = 175 \mu\text{m}$ ). **f**, Maximum fluorescence intensity along the streams measured for **e** as a function of  $x$  and  $y$ .

corresponding Debye length  $\lambda_D$  of 8.4 nm), where electrostatic interactions become prominent<sup>29,30,42</sup>, separation of lectin and streptavidin was clearly achieved, with two distinct streams visible under a horizontal field  $E_x = 250 \text{ V cm}^{-1}$  and vertical field  $E_y = 75 \text{ V cm}^{-1}$ . Streptavidin is more negatively charged at pH 9.6 compared to lectin owing to its lower pI value, and therefore streptavidin experiences greater repulsion during the jump across the nanofilter constriction<sup>29</sup>, leading to a lower jump passage rate  $P_x$  and a smaller deflection angle  $\theta$  (Fig. 5e). The stream deflection angles of streptavidin and lectin were about  $7.44^\circ$  and  $28.50^\circ$ , respectively, and the resolution values  $R_s$ , at 0.9 mm and 5 mm (extrapolated) from the injection point, are 0.32 and 1.96, respectively, indicating baseline resolution at the bottom of the ANA.

## DISCUSSION

We have observed direct experimental evidence of an unambiguous transition between Ogston sieving and entropic trapping in the ANA. The trajectories of different-sized DNA molecules are consistent with either Ogston sieving or entropic trapping (Fig. 6a). Crossover from Ogston sieving to entropic trapping occurs between 1,000 bp and 2,000 bp, which is concurrent with the transition from DNA rod-like conformation to coiled conformation and is consistent with observations in one-dimensional nanofilter arrays<sup>31</sup>. No saturation plateau was observed for entropic trapping in the ANA, in contrast to the one-dimensional nanofilter array<sup>31</sup>, indicating possible separation of long DNA in the ANA over an even broader size range. This different observation might be attributed to the more complex structural geometry of the ANA. In addition, the

two-dimensional anisotropic energy landscapes of the ANA are modulated by the two independent orthogonal fields  $E_x$  and  $E_y$ . Therefore, the local nanofilter jump dynamics of biomolecules is critically different from that in the one-dimensional nanofilter array. It is largely unknown how our understanding of the local nanofilter jump dynamics in the one-dimensional nanofilter array may be applied to the ANA. The effects of the two actively modulated orthogonal fields as well as all the ANA structural parameters need to be considered for a quantitative understanding of the different separation modes.

From the fluorescence intensity profile of Fig. 3b, the coefficients of variation (CVs) for the 150 bp, 300 bp and 500 bp DNA stream profiles are 8.6, 6.0 and 4.5%, respectively. Therefore, the size selectivity of the ANA in the Ogston sieving regime is about 5 nm (corresponding to the end-to-end distance of 20 bp DNA). The separation efficiency of the ANA can be further characterized by the effective peak capacity  $n_c$ , which defines the maximum number of separated streams that fit into the space provided by the separation<sup>39</sup>. Figure 6b shows the dependence of  $n_c$  on the horizontal field  $E_x$  for Ogston sieving, entropic trapping and electrostatic sieving. All the effective peak capacity curves initially increased quickly with  $E_x$  and then levelled off. This asymptotic behaviour of  $n_c$  can be largely attributed to the stream widening with increased  $E_x$ , which cancels out the increased lateral separation between the streams. The effective peak capacity  $n_c$  can be improved by increasing the separation distance. An optimized ANA structure with a gradient of decreasing constriction size along the positive  $x$  direction (an equivalent 'gradient gel') should also provide better resolution and separate proteins over a wider molecular weight range, similar to the effect of gradient-SDS gels

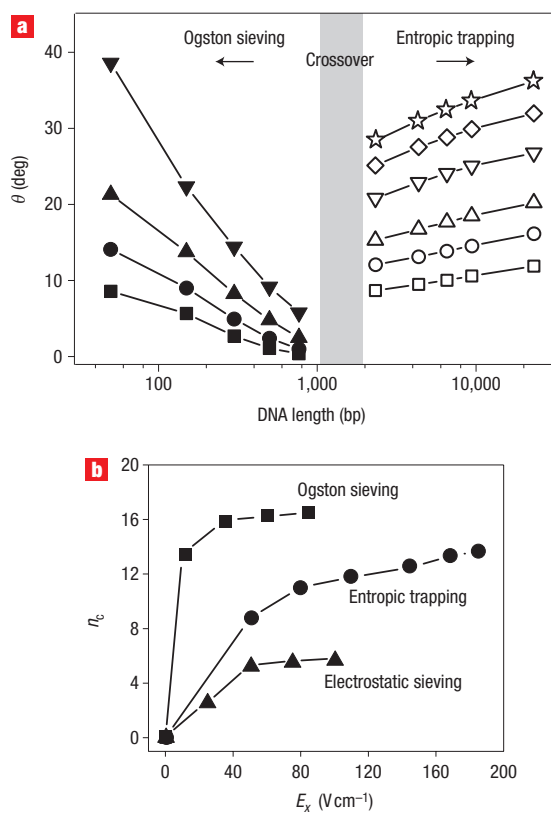


**Figure 6** Ogston sieving, entropic trapping and electrostatic sieving of DNA and proteins in the ANA. **a**, Stream deflection angle  $\theta$  as a function of DNA length. Left side (Ogston sieving):  $E_y = 25 \text{ V cm}^{-1}$  and  $E_x = 10 \text{ V cm}^{-1}$  (■),  $35 \text{ V cm}^{-1}$  (●),  $60 \text{ V cm}^{-1}$  (▲),  $85 \text{ V cm}^{-1}$  (▼). Right side (entropic trapping):  $E_y = 100 \text{ V cm}^{-1}$  and  $E_x = 50 \text{ V cm}^{-1}$  (□),  $80 \text{ V cm}^{-1}$  (○),  $110 \text{ V cm}^{-1}$  (△),  $145 \text{ V cm}^{-1}$  (▽),  $170 \text{ V cm}^{-1}$  (◇),  $185 \text{ V cm}^{-1}$  (☆). The  $\pm$ s.d. values of  $\theta$  derived from the stream half-width are all less than  $1^\circ$ , so statistical error bars for  $\theta$  are not plotted. **b**, Dependence of the effective peak capacity  $n_c$  on  $E_x$ . For Ogston sieving (■),  $E_y = 25 \text{ V cm}^{-1}$ ; for entropic trapping (●),  $E_y = 100 \text{ V cm}^{-1}$ ; for electrostatic sieving (▲),  $E_y = 50 \text{ V cm}^{-1}$ .

for protein separation<sup>1,43</sup>. Incorporating gate electrodes on the nanofilter walls can allow for additional active adjustment of the surface potential, thus introducing a new degree of control to enhance electrostatic sieving across the nanofilter<sup>44,45</sup>.

Other regular sieving structures for continuous-flow sorting of long DNA molecules and microspheres have been reported recently<sup>10–18</sup>, however, none of these techniques has demonstrated the separation of smaller physiologically relevant macromolecules, such as proteins, as we report here. The ANA also represents a significant advance compared with our earlier work in one-dimensional nanofilter arrays, because the continuous-flow operation of the ANA permits continuous harvesting of the subset of biomolecules of interest, which can enhance the specificity and sensitivity for downstream biosensing and detection. This advantage is highly desirable for integrated bioanalysis microsystems because of the higher sample throughput required. In addition, separation speed and resolution in one-dimensional nanofilter arrays cannot both be enhanced without compromising one another<sup>24</sup>, but in the ANA, they are mainly modulated, respectively, by the two independent fields  $E_x$  and  $E_y$ . Therefore, careful regulation of both  $E_x$  and  $E_y$  can always achieve rapid separation, with concurrent high resolution.

The designed structural anisotropy of the ANA is essential for continuous-flow separation. Continuous-flow separation through the ANA should be applicable to any interaction mechanism (size, charge or hydrophobicity based) along the orthogonal  $x$  direction that can lead to differential transport across the nanofilters. Its high-resolution separation and ease of sample collection may prove useful for preparative separation of complex biological samples, which has promising implications for proteomic research and biomarker discovery<sup>46,47</sup>. The sample throughput of the ANA can be further scaled up by parallelism using multi-device processing. We believe that the ANA can be used as a generic sieving structure to separate other particles of interest having nanoscale dimensions, including nanoparticles and nanowires, viruses and cell organelles. In addition, we envisage that it should be possible to develop anisotropic gel- or membrane-based large-scale biomolecule separation systems operating in the continuous-flow mode through the introduction of structural anisotropy by either photo-patterning anisotropic gel structures or stacking membranes in layers<sup>48</sup>.

In summary, we have designed and implemented a novel anisotropic nanofluidic sieving structure that can efficiently separate biologically relevant macromolecules within broad size ranges. The designed structural anisotropy causes different sized or charged macromolecules to follow distinct trajectories consistent with either Ogston sieving, entropic trapping or electrostatic sieving. We have successfully demonstrated high-resolution continuous-flow separation of a wide range of DNA fragments (between 50 bp and 23,000 bp) and proteins (between 11 kDa and 400 kDa) in just a few minutes. By virtue of its separation efficiency, ease of sample recovery and high throughput enabled by its continuous-flow operation, the ANA holds great promise as an integrated biomolecule sample preparation and analysis system.

## METHODS

### DEVICE DESIGN, FABRICATION AND METROLOGY

The shallow and deep regions of the ANA, as well as the microfluidic channels, were defined and etched into a Si wafer using photolithography and reactive-etching techniques. A  $5\times$  reduction step-and-repeat projection stepper (Nikon NSR2005i9, Nikon Precision) was used for patterning. KOH etching was performed at  $80^\circ\text{C}$  to etch through the wafer to creating buffer access holes. A 500-nm thermal oxide layer was grown to provide electrical isolation between the conductive Si substrate and the buffer solution. Finally, the device was sealed by bonding a Pyrex wafer on the front surface of the Si wafer. The bonded wafers were cut by dicesaw into individual devices for channel filling and separation experiments. The depths of the shallow and deep regions of the ANA were measured with a surface profilometer (Prometrix P-10, KLA-Tenco) before the anodic bonding process. The depths and surface uniformity of the nanofilter shallow regions were further checked by imaging the cross-section of the nanofilter with a scanning electron microscopy (JEOL6320FV, JEOL USA) after anodic bonding.

### SAMPLE PREPARATION

The PCR marker as well as  $\lambda$  DNA–Hind III digest (New England BioLabs) were labelled with the intercalating fluorescence dye YOYO-1 (Molecular Probes) in TBE  $5\times$  buffer. The dye-to-DNA base-pair ratio was about 1:2 and the final DNA concentration was about  $42.18 \mu\text{g ml}^{-1}$  (PCR) and  $104 \mu\text{g ml}^{-1}$  ( $\lambda$  DNA–Hind III digest). Proteins were dissolved in either TBE  $5\times$  or TBE  $0.05\times$  buffer, and the solution pH was further adjusted to 9.6 by addition of potassium hydroxide (Sigma-Aldrich). The following commercially available proteins and protein-conjugates were investigated: fluorescent B-phycoerythrin (Alexis Biochemicals), Alexa Fluor 488 conjugated fibrinogen and streptavidin (both from Molecular Probes), and fluorescein isothiocyanate (FITC) conjugated lectin from *Lens culinaris* (lentil) (Sigma-Aldrich). The final concentration of each protein sample in the mixture was about  $0.1\text{--}0.2 \text{ mg ml}^{-1}$ , except for lectin ( $0.2\text{--}0.4 \text{ mg ml}^{-1}$ ) owing to its lower fluorescence signal. For SDS–protein experiments, Alexa Fluor 488 conjugated cholera toxin subunit B was purchased from Molecular Probes.  $\beta$ -galactosidase

from *E. coli* was obtained from Sigma, and was custom-labelled with Alexa Fluor 488 by Molecular Probes. The complete denaturation of both proteins was performed by adding SDS (Sigma-Aldrich) and dithiothreitol (DTT, Sigma-Aldrich). The SDS–DTT protein mixture contained 2 wt% SDS and 0.1 M DDT, and was treated in an 80 °C water bath for 10 min. The resultant SDS–protein complex solutions were mixed and further diluted in TBE 5× buffer. The final SDS–protein complex sample solution contained 15.1 μg ml<sup>-1</sup> cholera toxin subunit B, 90.9 μg ml<sup>-1</sup> β-galactosidase, 0.1 wt% SDS and 5 μM DTT.

### SEPARATION

The ANA was filled with TBE 5× buffer for size-based DNA and protein separation and TBE 0.05× for charged-based protein separation, respectively. Additional 0.1 wt% SDS was added to TBE 5× buffer for SDS–protein experiments. In all experiments, DNA and SDS–protein complexes followed the direction of electrophoresis (owing to diminished electro-osmosis under high buffer ionic strength), but proteins under native conditions followed the direction of electro-osmosis (presumably owing to their lower net charge compared with DNA and therefore less strongly experienced electrophoretic drag). An inverted epi-fluorescence microscope (IX-71, Olympus) equipped with a thermoelectrically cooled CCD camera (Sensicam QE, Cooke) was used for fluorescence imaging, and a 100 W mercury lamp (Chiu Technical) was used for illumination. B-phycoerythrin was visualized with a Texas Red filter set (excitation, 562 nm; emission, 624 nm; Semrock), whereas all the other biomolecules were observed using a FITC filter set (excitation, 482 nm; emission, 536 nm; Semrock). The images were analysed with image processing software from IPLab (Scanalytics, BD Bioscience).

### SIZE SELECTIVITY, RESOLUTION AND PEAK CAPACITY

The CV of biomolecules of molecular weight  $m$  is defined as  $\sigma_m/m \times 100\%$ , where  $\sigma_m$  is the standard deviation ( $\pm$ s.d.) of  $m$ . When used as a measure for size selectivity, CV is calculated according to  $CV = \sigma_m/m = [(dm/d\theta)\sigma_\theta]/m$ , where  $\theta$  is the measured deflection angle, as a function of  $m$ , and  $\sigma_\theta$  is  $\pm$ s.d. of the deflection angle derived from the stream half-width. The effective peak capacity  $n_c$  is calculated based on some specified separation resolution value  $R_s$  of adjacent streams. Separation resolution  $R_s$  between two streams (streams 1 and 2) is defined as  $R_{s,12} = 0.5 \times \Delta x/(\sigma_1 + \sigma_2)$ , where  $\Delta x$  is the spatial distance between the two streams, and  $\sigma_1$  and  $\sigma_2$  are  $\pm$ s.d. of the stream widths. In the ANA, the effective peak capacity  $n_c$  for adjacent streams separated at  $R_s = 1$  is calculated as  $n_c = [5,000(\tan \theta_n - \tan \theta_1) + 2\bar{\sigma}_w]/(4\bar{\sigma}_w)$ , where  $\theta_1$  and  $\theta_n$  denote the smallest and largest stream deflection angles, respectively,  $\bar{\sigma}_w$  is the mean of the  $\pm$ s.d. of the stream widths, and 5,000 μm is the width of the rectangular ANA. For all the electropherograms measured, we have used gaussian functions for fitting to determine the means (the maximum intensity) as well as the stream widths. Please note that, owing to the low signal-to-background ratio, the separation resolution for electrostatic sieving of proteins at the bottom of the ANA is calculated by linearly extrapolating the stream separation distance and stream width along the streams.

Received 13 October 2006; revised 24 November 2006; accepted 15 December 2006; published 5 February 2007.

### References

- Scopes, R. K. *Protein Purification, Principles and Practice* 3rd edn (Springer-Verlag, New York, 1993).
- Giddings, J. C. *Dynamics of Chromatography. Part 1. Principles and Theory* (Marcel Dekker, New York, 1965).
- Slater, G. W., Mayer, P. & Drouin, G. Migration of DNA through gels. *Methods Enzymol.* **270**, 272–295 (1996).
- Viovy, J.-L. Electrophoresis of DNA and other polyelectrolytes: physical mechanisms. *Rev. Mod. Phys.* **72**, 813–872 (2000).
- Woolley, A. T. & Mathies, R. A. Ultra-high-speed DNA fragment separations using microfabricated capillary array electrophoresis chips. *Proc. Natl Acad. Sci. USA* **91**, 11348–11352 (1994).
- Yao, G. et al. SDS capillary gel electrophoresis of proteins in microfabricated channels. *Proc. Natl Acad. Sci. USA* **96**, 5372–5377 (1999).
- Callewaert, N. et al. Total serum protein N-glycome profiling on a capillary electrophoresis-microfluidics platform. *Electrophoresis* **25**, 3128–3131 (2004).
- Liu, L., Li, P. & Asher, S. A. Entropic trapping of macromolecules by mesoscopic periodic voids in a polymer hydrogel. *Nature* **397**, 141–144 (1999).
- Nykypanchuk, D., Strey, H. H. & Hoagland, D. A. Brownian motion of DNA confined within a two-dimensional array. *Science* **297**, 987–990 (2002).
- Volkmut, W. D. & Austin, R. H. DNA electrophoresis in microlithographic arrays. *Nature* **358**, 600–602 (1992).
- Turner, S. W., Perez, A. M., Lopez, A. & Craighead, H. G. Monolithic nanofluid sieving structures for DNA manipulation. *J. Vac. Sci. Technol. B* **16**, 3835–3840 (1998).
- Han, J. & Craighead, H. G. Separation of long DNA molecules in a microfabricated entropic trap array. *Science* **288**, 1026–1029 (2000).

- Huang, L. R. et al. A DNA prism: high speed continuous fractionation of large DNA molecules. *Nature Biotechnol.* **20**, 1048–1051 (2002).
- Baba, M. et al. DNA size separation using artificially nanostructured matrix. *Appl. Phys. Lett.* **83**, 1468–1470 (2003).
- Kaji, N. et al. Separation of long DNA molecules by quartz nanopillar chips under a direct current electric field. *Anal. Chem.* **76**, 15–22 (2004).
- Chou, F. et al. Sorting by diffusion: an asymmetric obstacle course for continuous molecular separation. *Proc. Natl Acad. Sci. USA* **96**, 13762–13765 (1999).
- van Oudenaarden, A. & Boxer, S. G. Brownian ratchets: molecular separation in lipid bilayers supported on patterned arrays. *Science* **285**, 1046–1048 (1999).
- Huang, L. R., Cox, E. C., Austin, R. H. & Sturm, J. C. Continuous particle separation through deterministic lateral displacement. *Science* **304**, 987–990 (2004).
- Austin, R. H. et al. Ratchets: the problems with boundary conditions in insulating fluids. *Appl. Phys. A* **75**, 279–284 (2002).
- Huang, L. R. et al. Role of molecular size in ratchet fractionation. *Phys. Rev. Lett.* **89**, 178301 (2002).
- Fu, J. & Han, J. Continuous-flow biomolecule separation through patterned anisotropic nanofluidic sieving structure. *Proc. Micro. Total Anal. Sys.* **1**, 519–521 (2006).
- Ogston, A. G. The spaces in a uniform random suspension of fibres. *Trans. Faraday Soc.* **54**, 1754–1757 (1958).
- Rodbard, D. & Chrambach, A. Unified theory for gel electrophoresis and gel filtration. *Proc. Natl Acad. Sci. USA* **65**, 970–977 (1970).
- Fu, J., Mao, P. & Han, J. Nanofilter array chip for fast gel-free biomolecule separation. *Appl. Phys. Lett.* **87**, 263902 (2005).
- Muthukumar, M. & Baumgärtner, A. Effects of entropic barriers on polymer dynamics. *Macromolecules* **22**, 1937–1941 (1989).
- Smisek, D. L. & Hoagland, D. A. Electrophoresis of flexible macromolecules: evidence for a new mode of transport in gels. *Science* **248**, 1221–1223 (1990).
- Rousseau, J., Drouin, G. & Slater, G. W. Entropic trapping of DNA during gel electrophoresis: effect of field intensity and gel concentration. *Phys. Rev. Lett.* **79**, 1945–1948 (1997).
- Han, J., Turner, S. W. & Craighead, H. G. Entropic trapping and escape of long DNA molecules at submicron size constriction. *Phys. Rev. Lett.* **83**, 1688–1691 (1999).
- Smith, F. G. & Deen, W. M. Electrostatic effects on the partitioning of spherical colloids between dilute bulk solution and cylindrical pores. *J. Colloid Interface Sci.* **91**, 571–590 (1983).
- Deen, W. M. Hindered transport of large molecules in liquid-filled pores. *AIChE J.* **33**, 1409–1425 (1987).
- Fu, J., Yoo, J. & Han, J. Molecular sieving in periodic free-energy landscapes created by patterned nanofilter arrays. *Phys. Rev. Lett.* **97**, 018103 (2006).
- Giddings, J. C., Kucera, E., Russell, C. P. & Myers, M. N. Statistical theory for the equilibrium distribution of rigid molecules in inert porous networks. Exclusion chromatography. *J. Phys. Chem.* **72**, 4397–4408 (1968).
- Slater, G. W., Gratton, Y., Kenward, M., McCormick, L. & Tessier, F. Deformation, stretching, and relaxation of single-polymer chains: fundamentals and examples. *Soft Mater.* **1**, 365–391 (2003).
- Schoch, R. B., Bertsch, A. & Renaud, P. pH-controlled diffusion of proteins with different pI values across a nanochannel on a chip. *Nano Lett.* **6**, 543–547 (2006).
- Huang, L. R. et al. Generation of large-area tunable uniform electric fields in microfluid arrays for rapid DNA separation. *Tech. Dig. Int. Elect. Dev. Mtg.* 363–366 (2002).
- Lide, D. R. *CRC Handbook of Chemistry and Physics* edn 87 (Taylor and Francis, Boca Raton, 2007).
- Hagerman, P. J. Flexibility of DNA. *Annu. Rev. Biophys. Biophys. Chem.* **17**, 265–286 (1988).
- Rubenstein, M. & Colby, R. H. *Polymer Physics* (Oxford, New York, 2003).
- Giddings, J. C. *Unified Separation Science* (Wiley, New York, 1991).
- Smith, D. E., Perkins, T. T. & Chu, S. Dynamical scaling of DNA diffusion coefficients. *Macromolecules* **29**, 1372–1373 (1996).
- Nakanishi, K., Sakiyama, T. & Imamura, K. On the adsorption of proteins on solid surfaces, a common but very complicated phenomenon. *J. Biosci. Biog.* **91**, 233–244 (2001).
- Schoch, R. B. *Transport Phenomena in Nanofluidics: From Ionic Studies to Proteomic Applications*. PhD Thesis No. 3538, EPFL, Lausanne (2006).
- Margolis, J. & Kenrick, K. G. Polyacrylamide gel-electrophoresis across a molecular sieve gradient. *Nature* **214**, 1334–1336 (1967).
- Karnik, R., Castelino, K. & Majumdar, A. Field-effect control of protein transport in a nanofluidic transistor circuit. *Appl. Phys. Lett.* **88**, 123114 (2006).
- Eijkel, J. C. T. & van den Berg, A. Nanotechnology for membranes, filters and sieves. *Lab. Chip* **6**, 19–23 (2006).
- Wulfkuhle, J. D., Liotta, L. A. & Petricoin, E. F. Proteomic applications for the early detection of cancer. *Nat. Rev. Cancer* **3**, 267–275 (2003).
- Righetti, P. G., Castagna, A., Herbert, B., Reymond, F. & Rossier, J. S. Prefractionation techniques in proteome analysis. *Proteomics* **3**, 1397–1407 (2003).
- Fu, J. & Han, J. Continuous biomolecule separation in a nanofilter structure. US Patent P-8195-USP, priority date 5 October 2006.

### Acknowledgements

We acknowledge financial support from NIH (EB005743), the DuPont–MIT Alliance, NSF (CTS-0347348) and Singapore–MIT Alliance (SMA-II, CE Program). We thank P. Mao for helping take the scanning electron microscopy images and J. Yoo for contributing to the experimental setup. We acknowledge valuable comments on and suggestions for the manuscript by P. Doyle, H. Bow and C. Rothman. The MIT Microsystems Technology Laboratories are acknowledged for support in fabrication. Supplementary information accompanies this paper on [www.nature.com/naturenanotechnology](http://www.nature.com/naturenanotechnology). Correspondence and requests for materials should be addressed to J.H.

### Author contributions

J.F. and J.H. conceived and initiated the ANA concept and J.F. designed and fabricated the ANA device. J.F. conceived and performed experiments with short DNA, long DNA and denatured proteins. R.B.S. conceived and performed experiments with native proteins. J.F. and R.B.S. analysed the data. A.L.S. performed gel analysis and J.F. and J.H. developed the theoretical model. J.F. and R.B.S. wrote the manuscript and J.H. and S.R.T. supervised the project.

### Competing financial interests

The authors declare that they have no competing financial interests.

Reprints and permission information is available online at <http://npg.nature.com/reprintsandpermissions/>